Streamwise evolution of the entrainment in a steady two-dimensional bluff-body wake

Daniela Tordella†
Dipartimento di Ingegneria Aeronautica e Spaziale, Politecnico di Torino, 10129 Torino, Italy

Stefania Scarsoglio
Scuola di Dottorato, Politecnico di Torino, 10129 Torino, Italy

Abstract. An asymptotic representation for entrainment in a two-dimensional steady wake behind a circular cylinder is presented. The Reynolds number R ranges from 20 to 100. The representation is obtained from an asymptotic Navier-Stokes solution that includes the region of the wake where the non-parallelism of the streamlines is not yet negligible.

The entrainment is determined as the flow rate variation in the streamwise direction. It is maximum at the beginning of the intermediate region just downstream of the symmetric counter rotating attached eddies. Moving downstream, it decreases continuously to zero, which is the asymptotic value in the far field.

The entrainment increases with the Reynolds number. In terms of the normalized volumetric flow rate, the spatial evolution of the entrainment depends on the Reynolds number up to a distance of almost 20 body scales. Afterwards, the Reynolds dependence becomes weak. In the R range here considered, the entrainment can be considered negligible at a normalized distance from the body in between $50 - 60$, that is, a distance value of the same order of magnitude of R. This result is in agreement with the scaling often adopted in wake stability studies to represent the slow spatial variation in a multiscaling framework.

Keywords: Entrainment, asymptotic expansions, 2D wake, Navier-Stokes solution

1. Introduction

The dynamics of entrainment and mixing is of considerable interest in engineering applications such as pollutant dispersal or combustion, but it is also of great relevance in geophysical and atmospherical situations. In all these instances, flows tend to be complex. In most cases entrainment is a time dependent multistage process both in the laminar or turbulent regime of motion.

The entrainment of an external fluid in a shear flow is a convective-diffusive process which is ubiquitous when the Reynolds number is greater than a few decades. It is a key phenomenon associated to the lateral momentum transport in flows which evolve about a main spatial direction. However, quantitative data concerning the entrainment

† daniela.tordella@polito.it

spatial evolution are not very frequent in literature and are difficult to determine experimentally. Quantitative experimental observations are very cumbersome to obtain either in the laboratory or in the numerical simulation context. In some cases, as for instance fluid entrainment by isolated vortex rings, theoretical studies (Maxworthy 1972, [1]) predate experimental observations (Baird, Wairegi and Loo 1977, [2]; Müller and Didden 1980, [3]; Dabiri and Gharib 2004, [4]).

It is interesting to note that more attention has been paid to complex unsteady and highly turbulent configurations in literature than to their fundamentally simpler steady counterparts.

In unsteady situations, entrainment is believed to consist of repeated cycles of viscous diffusion and circulatory transport. In turbulent flows, a sequence of processes is observed, where the exterior fluid is first ingested by the highly stretched and twisted interior turbulent motion (large-scale stirring) and is then mixed to the molecular level by the action of the small-scale velocity fluctuations, see for instance the recent experimental works carried out on free jets by Grinstein 2001, [5] or on a plane turbulent wake by Kopp, Giralt and Keffer 2002, [6].

In steady laminar shear flows, the stretching dynamics is generally absent (as in 2D flows) or is close to its onset. In this case, the entrainment is ruled out by the balance between the longitudinal and lateral nonlinear convective transport and the mainly lateral molecular diffusion.

In this paper, we consider the steady flow past a circular cylinder, which is the quintessential bluff body. We deduce the entrainment as the longitudinal volume flow rate variation using a matched Navier-Stokes asymptotic solution determined in terms of inverse powers of the space variables (Belan and Tordella 2002, [7]; Tordella and Belan 2003, [8]), see Section 2. The solution was obtained by recognizing the existence of a longitudinal intermediate region, which introduces the adoption of the thin shear layer hypothesis and supports a differentiation of the behaviour of the intermediate flow with respect to its infinite asymptotics. The general n-order expansion term for the flow rate and the entrainment is given in Section 2, whilst the first four orders of the expansion coefficients are listed in Subsection 2.1.

The streamwise behaviour of the entrainment is presented in Section 3. Two possible lateral integration limits are discussed: - the displacement thickness and - the wake thickness, which is explicited through the introduction of a threshold ϵ. The concluding remarks are given in Section 4.

2. Basic formulation

For an incompressible, viscous flow behind a bluff body, the adimensional continuity and Navier-Stokes equations are expressed as

$$u\partial_x u + v\partial_y u + \partial_x p = R^{-1}\nabla^2 u \quad (1)$$

$$u\partial_x v + v\partial_y v + \partial_y p = R^{-1}\nabla^2 v \quad (2)$$

$$\partial_x u + \partial_y v = 0 \quad (3)$$

where (x, y) are the adimensional longitudinal and normal coordinates, (u, v) the adimensional components of the velocity field, p the pressure and R the Reynolds number. The physical quantities involved in the adimensionalization are the length D of the body that generates the wake, the density ρ and the velocity U of the free stream, see the flow schematic in fig. 1. The Reynolds number is defined as $R = \rho UD/\mu$, where μ is the dynamic viscosity of the fluid.
The velocity field for the intermediate region of the $2D$ steady wake behind a circular cylinder is determined using an asymptotic Navier-Stokes expansion [8]. The solution is obtained by matching an inner solution - a Navier-Stokes expansion in negative powers of the inverse of the longitudinal coordinate $(x^{-n/2}, n = 0, 1, 2, ...)$ - and an outer solution, which is a Navier-Stokes asymptotic expansion in powers of the inverse of the distance from the body. The physical quantities involved in the matching criteria are the vorticity, the longitudinal pressure gradients generated by the flow and the transversal velocities. Here we approximate the basic wake flow components with the inner flow solution

$$u(x, y) = \phi_0(x, y) + \phi_1(x, y)x^{-1/2} \ldots = \sum_{n=0}^{N} \phi_n(x, y)x^{-n/2} \quad (4)$$

$$v(x, y) = \chi_0(x, y) + \chi_1(x, y)x^{-1/2} \ldots = \sum_{n=0}^{N} \chi_n(x, y)x^{-n/2} \quad (5)$$

The normalized volumetric flow rate Q can be defined as

$$\begin{aligned} Q(x) &= \frac{1}{2z_w\delta}\int_{-z_w}^{z_w}\int_0^{\delta} u(x, y)dydz \\ &= \frac{1}{2z_w\delta}\Big(\int_{-z_w}^{z_w}\int_0^{\delta} \phi_0(x, y)dydz + x^{-1/2}\int_{-z_w}^{z_w}\int_0^{\delta} \phi_1(x, y)dydz \\ &\quad + x^{-1}\int_{-z_w}^{z_w}\int_0^{\delta} \phi_2(x, y)dydz + \ldots\Big) \end{aligned}$$

$$= q_0(x) + q_1(x)x^{-1/2} + q_2(x)x^{-1} + \ldots = \sum_{n=0}^{N} q_n(x)x^{-n/2} \quad (6)$$

where $\delta = \delta(x, R)$ is a measure of the half inner wake thickness, z_w is an arbitrary spanwise length and

$$q_n(x) = \frac{1}{2z_w\delta}\int_{-z_w}^{z_w}\int_0^{\delta}\phi_n(x,y)dydz = \frac{1}{\delta}\int_0^{\delta}\phi_n(x,y)dy. \quad (7)$$

Since the wake is symmetric around the x coordinate, the adimensionalized longitudinal velocity u is integrated in the transversal direction between 0 and δ.

The wake width δ is a function of x and R and it can be defined in terms of the displacement thickness of the boundary-layer theory ([7], eq.(40))

$$\delta(x, R) = \frac{2}{1 - u(x, y = 0; R)}\int_0^{\infty}(1 - u(x, y; R))dy \quad (8)$$

If the wake width is approximated using the longitudinal velocity up to $n = 1$, $u(x, y) = \phi_0(x, y) + x^{-1/2}\phi_1(x, y) = C_0 - AC_1x^{-1/2}\mathrm{e}^{-Ry^2/(4x)}$, where C_0, C_1 are integration constants ($C_0 = 1, C_1 = 1$) and A is related to the drag coefficient ($A = \frac{1}{4}(R/\pi)^{1/2}c_D(R)$), see [7]–[8], one obtains

$$\delta(x, R) = \frac{2}{AC_1x^{-1/2}}\int_0^{\infty}(AC_1x^{-1/2}\mathrm{e}^{-Ry^2/(4x)})dy = 2\sqrt{\frac{\pi}{R}}x^{1/2}, \quad (9)$$

see fig. 2. The approximated asymptotic behavior $\delta \sim x^{1/2}$ can then be obtained.

The wake width can alternatively be defined by introducing the parameter ϵ, so that

$$|1 - u(x, y_w; R)| = \epsilon, \quad (10)$$

Thus, we can define the physical width y_w as the half-wake thickness where condition (10) is met, with $0 < \epsilon \leq 0.1$. At the $n = 1$ order, the wake width is

$$y_w(x; \epsilon, R) = \frac{2}{\sqrt{R}}[x\log(\frac{AC_1}{\epsilon\sqrt{x}})]^{1/2}, \quad (11)$$

see fig. 3, where the dependence on ϵ of the wake width is shown in parts (a, b) and where a comparison between definitions (8) and (10) is presented on the volumetric flow rate in parts (c, d).

The entrainment is the quantity that takes into account the volumetric flow rate variation in the streamwise direction, and is defined as $E(x) = \dfrac{dQ(x)}{dx}$. Using expansion (6), one obtains

$$\begin{aligned} E(x) &= \frac{dQ(x)}{dx} \\ &= \sum_{n=0}^{N} [t_n(x) - \frac{n-2}{2} q_{n-2}(x)] x^{-n/2} \\ &= \sum_{n=0}^{N} e_n(x) x^{-n/2} \end{aligned} \tag{12}$$

where

$$t_n(x) = \frac{dq_n(x)}{dx} = \frac{d}{dx}(\frac{1}{\delta}\int_0^{\delta} \phi_n(x,y)dy) \tag{13}$$

and where the sequence of the coefficients of the flow rate expansion (6) is enlarged to include the elements $q_{-2} = 0$ and $q_{-1} = 0$.

The expression for coefficients $\phi_n(x,y)$ [8] is

$$\phi_0(x,y) = C_0 = 1, \tag{14}$$

which satisfies the boundary condition on u as $x \to \infty$, and

$$\begin{aligned} \phi_n(x,y) &= A^n \mathrm{e}^{-Ry^2/(4x)} [C_n {}_1\mathrm{F}_1(\frac{1-n}{2}, \frac{1}{2}; \frac{Ry^2}{4x}) \\ &\quad + R\mathrm{Hr}_{n-1}(x,y) F_n(x,y)], \ n \geq 1. \end{aligned} \tag{15}$$

The integration constants C_n are determined by boundary and matching conditions between the inner and outer solutions [7]–[8], while the constant A is related to the drag coefficient ($A = \frac{1}{4}(R/\pi)^{1/2} c_D(R)$). Function ${}_1\mathrm{F}_1$ is the confluent hypergeometric function, $\mathrm{Hr}_{n-1}(x,y) = \mathrm{H}_{n-1}(\frac{1}{2}\sqrt{\frac{R}{x}}y)$, where H_n are Hermite polynomials, and

$$F_n(x,y) = \frac{1}{\sqrt{x}} \int_0^y \frac{\mathrm{e}^{R\zeta^2/(4x)}}{\mathrm{Hr}_{n-1}^2(x,\zeta) G_n(x,\zeta)} d\zeta \tag{16}$$

$$G_n(x,y) = A^{-n} \frac{1}{\sqrt{x}} \int_0^y M_n(x,\zeta) \mathrm{Hr}_{n-1}(x,\zeta) d\zeta \tag{17}$$

Function $M_n(x,y)$ is the sum of the non homogeneous terms of the general ordinary differential equation for ϕ_n, $n \geq 1$, obtained from the x component of the Navier-Stokes equation [7]–[8].

Once ϕ_n are known, coefficients χ_n can be obtained through the continuity equation, so that

$$\chi_0(x,y) = 0, \tag{18}$$

which satisfies the boundary condition on v as $x \to \infty$, and

$$\chi_n(x,y) = \frac{1}{2\sqrt{x}}[y\phi_{n-1}(x,y) + (n-2)\int_0^y \phi_{n-1}(x,\zeta)d\zeta], \ n \geq 1. \quad (19)$$

The entrainment $E(x)$ can thus be directly related to the transversal velocity through coefficients χ_n, as

$$e_n(x) = t_n(x) - \frac{n-2}{2}q_{n-2}(x) \quad (20)$$

with

$$t_n(x) = \sqrt{\frac{R}{\pi}}\frac{d}{dx}\{\int_0^\delta y^{-n}\int_0^y [\zeta^{n-1}\frac{\partial}{\partial\zeta}\chi_{n+1}(x,\zeta)]d\zeta dy\} \quad (21)$$

and

$$q_n(x) \ = \ \sqrt{\frac{R}{\pi}}\int_0^\delta y^{-n}\int_0^y [\zeta^{n-1}\frac{\partial}{\partial\zeta}\chi_{n+1}(x,\zeta)]d\zeta dy. \quad (22)$$

2.1. Expansion of the first four orders

Here we list in sequence the inner expansions for the streamwise velocity (4), the transversal velocity (5), the flow rate (6) and the entrainment (12) up to the fourth order. The explicit expressions are

$$\begin{aligned}
u(x,y) &= \phi_0(x,y) + \phi_1(x,y)x^{-1/2} \\
&\quad +\phi_2(x,y)x^{-1} + \phi_3(x,y)x^{-3/2} && (23)\\
v(x,y) &= \chi_0(x,y) + \chi_1(x,y)x^{-1/2} \\
&\quad +\chi_2(x,y)x^{-1} + \chi_3(x,y)x^{-3/2} && (24)\\
Q(x) &= q_0(x) + q_1(x)x^{-1/2} \\
&\quad +q_2(x)x^{-1} + q_3(x)x^{-3/2} && (25)\\
E(x) &= t_0(x) + t_1(x)x^{-1/2} \\
&\quad +t_2(x)x^{-1} + (t_3(x) - \frac{1}{2}q_1(x))x^{-3/2} && (26)
\end{aligned}$$

First order, n=0

$$\begin{aligned}
\phi_0(x,y) &= C_0 && (27)\\
\chi_0(x,y) &= 0 && (28)\\
q_0(x) &= 1 && (29)\\
t_0(x) &= 0 && (30)
\end{aligned}$$

with $C_0 = 1$.

Second order, n=1

$$\phi_1(x,y) = -AC_1 \mathrm{e}^{-Ry^2/(4x)} \tag{31}$$
$$\chi_1(x,y) = 0 \tag{32}$$
$$q_1(x) = -\frac{AC_1}{\delta}\int_0^\delta \mathrm{e}^{-Ry^2/(4x)}dy = -\frac{AC_1}{2}\mathrm{erf}(\sqrt{\pi}) \tag{33}$$
$$t_1(x) = -AC_1\frac{d}{dx}(\frac{1}{\delta}\int_0^\delta \mathrm{e}^{-Ry^2/(4x)}dy) = 0 \tag{34}$$

with $C_1 = 1$.

Third order, n=2

$$\begin{aligned}\phi_2(x,y) = &-\frac{1}{2}A^2\mathrm{e}^{-Ry^2/(4x)}[C_{21}\mathrm{F}_1(-\frac{1}{2},\frac{1}{2};\frac{Ry^2}{4x}) \\ &+\mathrm{e}^{-Ry^2/(4x)} + \frac{1}{2}\frac{y}{\sqrt{x}}\sqrt{\pi R}\mathrm{erf}(\frac{1}{2}\sqrt{\frac{R}{x}}y)]\end{aligned} \tag{35}$$
$$\chi_2(x,y) = -\frac{A}{2}\frac{y}{\sqrt{x}}\mathrm{e}^{-Ry^2/(4x)} \tag{36}$$
$$\begin{aligned}q_2(x) = &-\frac{A^2}{2\delta}\int_0^\delta\{\mathrm{e}^{-Ry^2/(4x)}[C_{21}\mathrm{F}_1(-\frac{1}{2},\frac{1}{2};\frac{Ry^2}{4x}) \\ &+\mathrm{e}^{-Ry^2/(4x)} + \frac{1}{2}\frac{y}{\sqrt{x}}\sqrt{\pi R}\mathrm{erf}(\frac{1}{2}\sqrt{\frac{R}{x}}y)]\}dy\end{aligned} \tag{37}$$
$$\begin{aligned}t_2(x) = &-\frac{A^2}{2}\frac{d}{dx}(\frac{1}{\delta}\int_0^\delta\{\mathrm{e}^{-Ry^2/(4x)}[C_{21}\mathrm{F}_1(-\frac{1}{2},\frac{1}{2};\frac{Ry^2}{4x}) \\ &+\mathrm{e}^{-Ry^2/(4x)} + \frac{1}{2}\frac{y}{\sqrt{x}}\sqrt{\pi R}\mathrm{erf}(\frac{1}{2}\sqrt{\frac{R}{x}}y)]\}dy)\end{aligned} \tag{38}$$

with $C_2 = -2.75833 + 0.21237 \cdot R - 0.00353 \cdot R^2 + 0.00002 \cdot R^3$.

Fourth order, n=3

$$\phi_3(x,y) = A^3\mathrm{e}^{-Ry^2/(4x)}(2 - R\frac{y^2}{x})[\frac{1}{2}C_3 - RF_3(x,y)] \tag{39}$$
$$\begin{aligned}\chi_3(x,y) = &-\frac{A^2}{2}\{C_2[-\frac{1}{2}\frac{1}{\sqrt{x}}\int_0^y[\mathrm{e}^{-R\zeta^2/(4x)}{}_1\mathrm{F}_1(-\frac{1}{2},\frac{1}{2};\frac{R\zeta^2}{4x})]d\zeta \\ &-\frac{1}{2}\frac{y}{\sqrt{x}}\mathrm{e}^{-Ry^2/(4x)}{}_1\mathrm{F}_1(-\frac{1}{2},\frac{1}{2};\frac{Ry^2}{4x})]\end{aligned}$$

$$-\frac{1}{2}\frac{y}{\sqrt{x}}\mathrm{e}^{-Ry^2/(2x)} - \sqrt{\frac{\pi}{2R}}\mathrm{erf}(\sqrt{\frac{R}{2x}}y)$$
$$+(\frac{1}{2}\sqrt{\frac{\pi}{R}} - \frac{\sqrt{\pi R}}{4}\frac{y^2}{x})\mathrm{e}^{-Ry^2/(4x)}\mathrm{erf}(\frac{1}{2}\sqrt{\frac{R}{x}}y) \quad (40)$$

$$q_3(x) = \frac{A^3}{\delta}\int_0^\delta \{\mathrm{e}^{-Ry^2/(4x)}(2 - R\frac{y^2}{x})$$
$$\times[\frac{1}{2}C_3 - RF_3(x,y)]\}dy \quad (41)$$

$$t_3(x) = A^3\frac{d}{dx}(\frac{1}{\delta}\int_0^\delta \{\mathrm{e}^{-Ry^2/(4x)}(2 - R\frac{y^2}{x})$$
$$\times[\frac{1}{2}C_3 - RF_3(x,y)]\}dy) \quad (42)$$

with $C_3 = -2.26605 + 0.15752 \cdot R - 0.00265 \cdot R^2 + 0.00001 \cdot R^3$.

3. Discussion of the results

The solutions in the form of the asymptotic expansions used to represent the inner steady symmetric flow behind the circular cylinder are plotted in figures 4 and 5 to highlight the combined effects of the R and the downstream spatial decay. The solutions were obtained under the thin shear layer and quasi-similarity hypotheses. Their validity is therefore limited to the middle and far portions of the field. In figures 4 and 5, the plots begin at $x = 5$, which is an average value, in the range of R here considered, of the distance from the body beyond which the thin shear layer model becomes relevant. This distance, nominally a function of the R (a decreasing function) and of the shape of the body, should be considered a free parameter. Its value, at fixed R can, in theory, be obtained by means of the matching with the pre-asymptotic flow. Both the origin and the near wake, which includes the symmetrical adherent vortices, fall outside the domain of the present analysis. Further limiting assumptions such as the Oseen successive approximations or the shape of the lateral asymptotics, were not used.

The asymptotic behaviour of these expansions in the lateral far field is very important to determine the entrainment spatial evolution. At finite values of x, the coefficient function ϕ for the streamwise velocity decays to zero as a Gaussian law for $n = 1$ and as a power law of exponent -2 for $n = 2$ and of exponent -3 for $n \geq 3$. The coefficient function χ for the cross-stream velocity goes to zero for $n = 0, 1$ and to a constant value for $n \geq 2$. This allows v to vanish as $x^{-3/2}$ for $x \to \infty$. When $x \to \infty$ this solution coincides with the

Gaussian representation given by the Oseen approximation. It can be concluded that, at Reynolds numbers as low as the first critical value and where the non-parallelism of the streamlines is not yet negligible, the division of the field into two basic parts - an inner vortical boundary layer flow and an outer potential flow - is spontaneously shown up to the second order of accuracy ($n = 1$). At higher orders in the expansion solution, the vorticity is first convected and then diffused in the outer field. This is the dynamical context in which the entrainment process takes place.

Figure 6 shows the volumetric flow rate $Q = Q(x, R)$ and the entrainment $E = E(x, R)$ obtained from expansions (6), (12). It can be observed that these quantities significantly depend on the flow control parameter up to a distance of nearly 20 body scales. In fact, at $x = 5$, by varying $R \in [20, 100]$, Q varies from 0.24 to 0.62, that is, an increase of R by a factor 5 produces an increase of Q by a factor ~ 2.5. However, this factor at $x \sim 22$ reduces to 1.1, see fig. 6a. An equivalent situation is observed for the entrainment, which is the derivative of the volumetric flow rate, see fig. 6b. By moving further downstream, the increase of Q and E with R continues to shrink to just a few percent at about $x \in [50 - 60]$. At this distance the volumetric flow rate is close to 90% of the far field unitary value. Correspondingly, the entrainment process is practically exhausted. It is interesting to observe that this distance happens to be of the same order of magnitude of R, which means that the scaling used in the multiscaling stability analysis to represent the slow time and space wake evolution - $\tau = \varepsilon t$ and $\xi = \varepsilon x$, where $\varepsilon = \dfrac{1}{R}$ - is linked to the exhaust of the entrainment process, that is, the units of the slow time and spatial scales are reached where the entrainment ends.

It is interesting to note that the trend shown by the entrainment is qualitatively close to the trend shown by the wave number and pulsation evolution of the dominant saddle–point of the zero order dispersion relation yielded by the nonparallel Orr-Sommerfeld stability analysis (Tordella, Scarsoglio and Belan 2006, [9]; Belan and Tordella 2006, [10]). In relation to this observation, we have highlighted the values of Q and E at $R = 50$ and 100 for which the instability becomes absolute in figure 6 (triangle and circle symbols). It should be noticed that the corresponding positions ($x \sim 10$) are close to the beginning of the intermediate wake where the spatial evolution is intense, but inside the region where the thin shear layer hypothesis is valid, a fact that *a posteriori* makes the use of the WKBJ method to study the stability in slowly varying flows self-consistent.

We close the results analysis with a short comment on the lateral integral scales that can be used to determine integral quantities such as the volumetric flow rate and the entrainment. An intuitive quantity in this regard is the wake width, which in order to be defined, needs the introduction of an arbitrary threshold, see in Section 2 equation (10) and figure 3. A choice of a very small threshold ϵ would be meaningless because it would imply a transversal length of integration going to infinity, which would not allow the finite flow rate variations associated to the momentum defect in the wake to be estimated. An alternative to the wake width is the displacement thickness, an integral quantity often used in the boundary layer theory and which is directly associated to the momentum defect in the wake, eq.(8). Figures 3 and 7 show that the results obtained using the displacement thickness are very close to the results obtained using a threshold equal to 0.01 (a position where the streamwise component of the velocity reaches 99% of the velocity of the external field). As known, this is a very popular value in boundary layer literature and engineering practice.

4. Conclusions

The entrainment distribution in the intermediate and far laminar two-dimensional wake behind a circular cylinder has been obtained in this work. The entrainment of external fluid is analytically determined as an asymptotic expansion, in terms of negative fractional powers of the longitudinal coordinate, using recent Navier-Stokes expansion solutions for the inner–field of the wake that successfully match an external Navier-Stokes field. The general n-order term of the expansion is explicitly obtained.

The entrainment is observed to be intense - the maximum of the distribution - downstream of the separation region where the two-symmetric standing eddies are situated. Here, the dependence on the Reynolds number is clear, the entrainment trebles when R is increased from 20 to 100. The subsequent downstream evolution presents a continuous decrement of the entrainment which, in the case of a wake flow, must go to zero in the far field. It can be observed that the decrease is almost accomplished for all the R here considered at an average distance from the body of $50 \sim 60$ diameters, which is a value of the same order of magnitude as the control parameter R. On the one hand, this indicates that the R dependence becomes weak when moving downstream. On the other hand, it confirms the validity of the scaling that is often adopted in wake stability studies carried out using the spatial and temporal multiscaling approach. In these studies, the

slow temporal and spatial scales τ, ξ are usually taken equal to $\tau = \varepsilon t$ and $\xi = \varepsilon x$, where $\varepsilon = \dfrac{1}{R}$. In the light of the present result, it can be concluded that $\tau \sim 1$, $\xi \sim 1$ are the physical scales that correspond to the downstream accomplishment of the entrainment process.

References

1. Maxworthy, T. The structure and stability of vortex rings. *J. Fluid Mech.*, 51: 15–32, 1972.
2. Baird, M. H. I., T. Wairegi and H. J. Loo. Velocity and momentum of vortex rings in relation to formation parameters. *Can. J. Chem. Engng.*, 55: 19–26, 1977.
3. Müller, E. A. and N. Didden. Zur erzeugung der zirkulation bei der bildung eines ringwirbels an einer dusenmundung. *Stroj. Casop.*, 31: 363–372, 1980.
4. Dabiri, J. O. and M. Gharib. Fluid entrainment by isolated vortex rings. *J. Fluid Mech.*, 511: 311–331, 2004.
5. Grinstein, F. F. Vortex dynamics and entrainment in rectangular free jets. *J. Fluid Mech.*, 437: 69–101, 2001.
6. Kopp, G. A., F. Giralt and J. F. Keffer. Entrainment vortices and interfacial intermittent turbulent bulges in a plane turbulent wake. *J. Fluid Mech.*, 469: 49–70, 2002.
7. Belan, M. and D. Tordella. Asymptotic expansions for two-dimensional symmetrical laminar wakes. *ZAMM*, 82 (4): 219–234, 2002.
8. Tordella, D. and M. Belan. A new matched asymptotic expansion for the intermediate and far flow behind a finite body. *Physics of Fluids*, 15 (7): 1897–1906, 2003.
9. Tordella, D., S. Scarsoglio and M. Belan. A synthetic perturbative hypothesis for multiscale analysis of convective wake instability. *Physics of Fluids*, 18 (5), 2006.
10. Belan, M. and D. Tordella. Convective instability in wake intermediate asymptotics. *J. Fluid Mech.*, 552: 127–136, 2006.

List of Captions

Fig. 1 - Sketch of the physical problem. Longitudinal velocity profiles (solid lines) and wake width δ (dashed lines) at $R = 60$ and at stations x = 7D , x = 17D.

Fig. 2 - Wake displacement thickness δ in (8)–(9) as a function of x for $R = 20, 40, 60, 80, 100$.

Fig. 3 - Wake width y_w, in (10)–(11), as a function of ϵ for $R = 20$, $R = 60$, $R = 100$ at $x = 15$ (part a) and $x = 60$ (part b). In parts (c, d) the volumetric flow rate Q is shown as a function of ϵ according to y_w definition (10)–(11) (solid lines) and δ definition (8)–(9) (dashed lines) for $R = 20$, $R = 60$, $R = 100$. Downstream stations $x = 15$ (c) and $x = 60$ (d).

Fig. 4 - Velocity profiles at the downstream stations $x = 20$, $x = 80$ and for $R = 20, 40, 60, 80$ and 100. Longitudinal velocity u: (a) $x = 20$, (b) $x = 80$, transversal velocity v: (c) $x = 20$, (d) $x = 80$.

Fig. 5 - Velocity profiles for $R = 30, 70$ plotted at stations $x = 10, 20, 40, 60, 80$ and 100. Longitudinal velocity u: (a) $R = 30$, (b) $R = 70$, transversal velocity v: (c) $R = 30$, (d) $R = 70$.

Fig. 6 - Downstream distribution of the volumetric flow rate Q (a) and entrainment E (b) for $R = 20, 40, 50, 60, 80$ and 100. Integration carried out using the δ wake width definition in (8)–(9). The triangle ($R = 50$) and the circle ($R = 100$) are values related to the wake regions where absolute instability occurs, according to a recent Orr-Sommerfeld spatio-temporal multiscale analysis (Tordella, Scarsoglio and Belan 2006, [9]; Belan and Tordella 2006, [10]).

Fig. 7 - (a) Volumetric flow rate Q and (b) entrainment E as a function of x for $R = 40$. Integration carried out using y_w wake width definition in (10)–(11), curves with $\epsilon = 10^{-6}, 10^{-4}, 10^{-2}, 10^{-1}$. The dashed lines represent Q and E obtained using the displacement thickness δ, in (8)–(9).

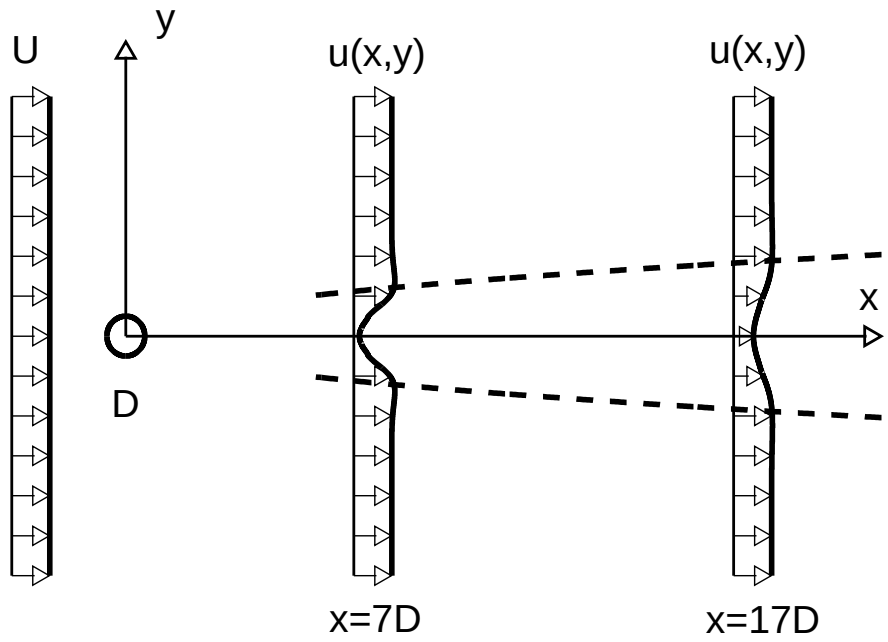

Figure 1. Tordella D. and S. Scarsoglio, Journal of Engineering Mathematics

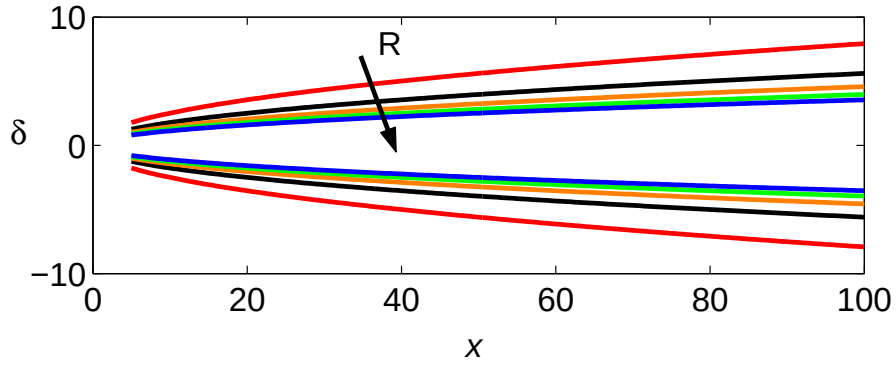

Figure 2. Tordella D. and S. Scarsoglio, Journal of Engineering Mathematics

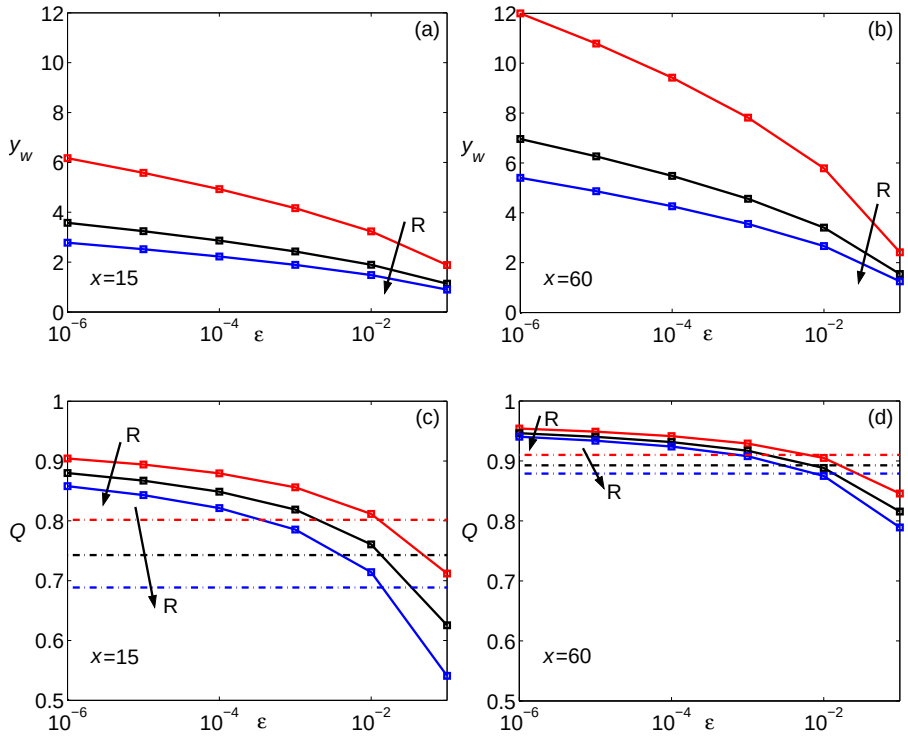

Figure 3. Tordella D. and S. Scarsoglio, Journal of Engineering Mathematics

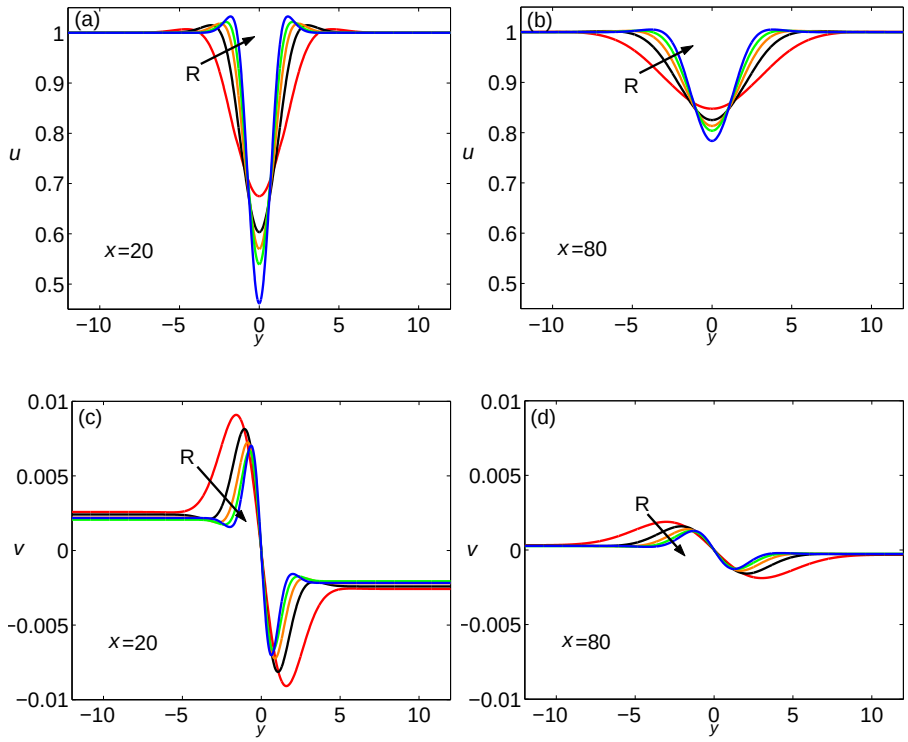

Figure 4. Tordella D. and S. Scarsoglio, Journal of Engineering Mathematics

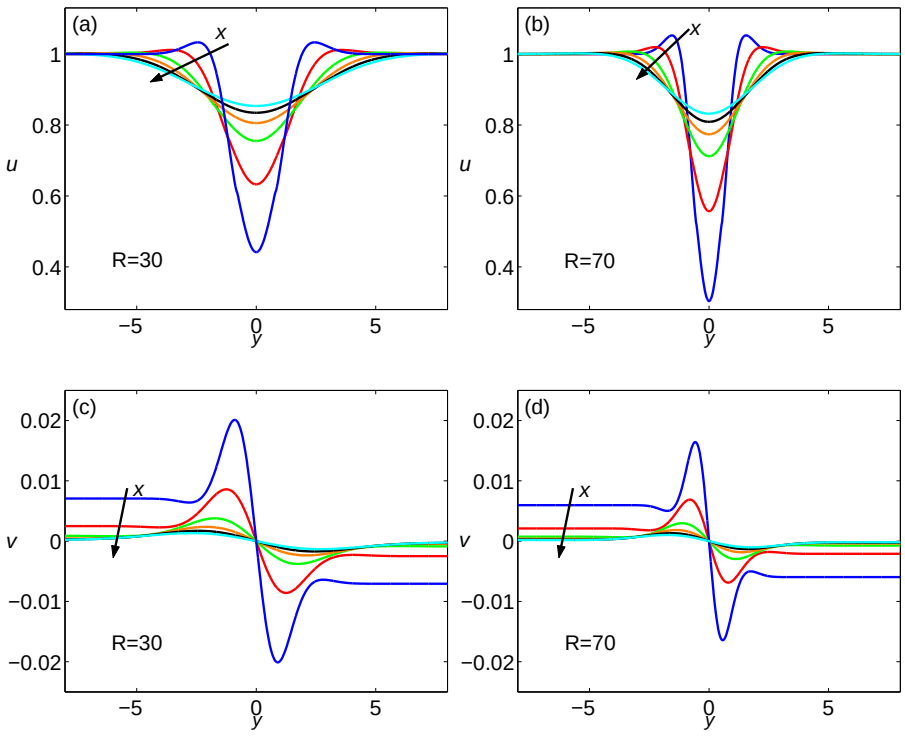

Figure 5. Tordella D. and S. Scarsoglio, Journal of Engineering Mathematics

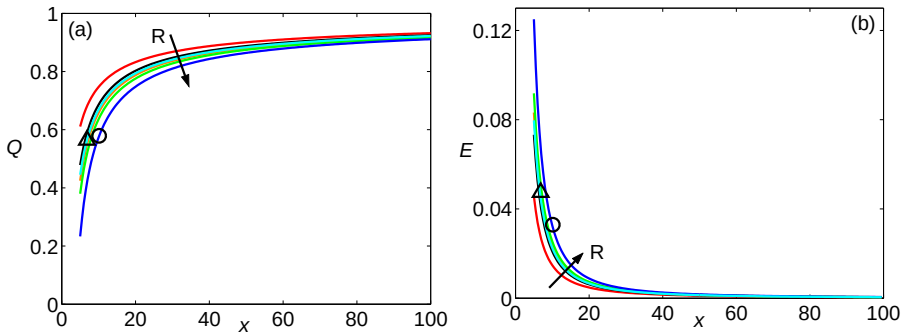

Figure 6. Tordella D. and S. Scarsoglio, Journal of Engineering Mathematics

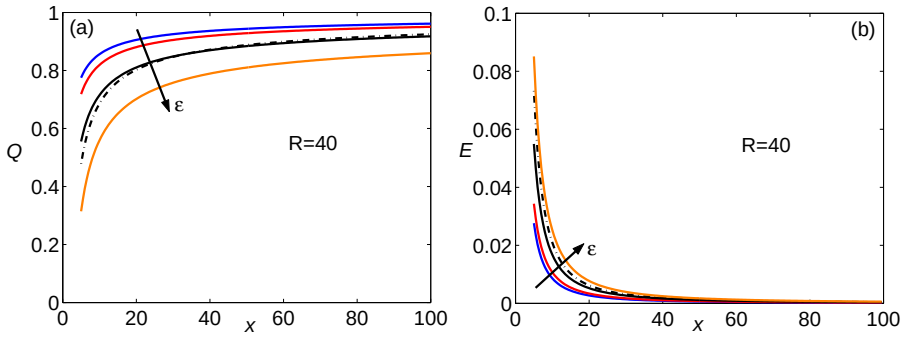

Figure 7. Tordella D. and S. Scarsoglio, Journal of Engineering Mathematics